

## Seasonal and Diurnal Variations of Ozone near the Mesopause from Observations of the 11.072-GHz Line

A. E. E. ROGERS

*MIT Haystack Observatory, Westford, Massachusetts*

M. LEKBERG

*Chelmsford High School, Chelmsford, Massachusetts*

P. PRATAP\*

*MIT Haystack Observatory, Westford, Massachusetts*

(Manuscript received 4 February 2009, in final form 8 June 2009)

### ABSTRACT

Ground-based observations of the 11.072-GHz line of ozone were made from January 2008 through January 2009. These observations provide an estimate of the diurnal and seasonal variations of ozone in the mesopause region. The 11-GHz line is more sensitive to the ozone at higher altitudes than ground observations of the 142-GHz line, because of the reduced Doppler line width. The observations show an increase in the volume mixing ratio of ozone above 80 km at night by more than a factor of 10 and a seasonal variation of about a factor of 2, which is consistent with the semiannual variations of atomic hydrogen in the mesopause region. The diurnal amplitude and rates of change of the mixing ratios at sunrise and sunset are compared with ground-based observations of the 142-GHz line and the observations of the Sounding of the Atmosphere using Broadband Emission Radiometry (SABER) instrument on the Thermosphere, Ionosphere, Mesosphere, Energetics and Dynamics (TIMED) satellite, as well as with a simplified chemical model of the creation and destruction of ozone in the mesopause region.

### 1. Introduction

The diurnal variations of ozone have been remotely sensed using ground-based radiometry by Wilson and Schwartz (1981) at 101.737 GHz and by Lobsiger and Künzi (1986) and Zommerfelds et al. (1989) at 142.175 GHz. In the case of millimeter wave lines, the thermal Doppler line width starts to dominate the pressure broadening at an altitude of about 75 km. The variation of line width with altitude allows the retrieval of the ozone volume mixing ratio (vmr) up to this altitude regime. We report observations using the microwave line of ozone at

11.072 454 5 GHz [Jet Propulsion Laboratory (JPL) catalog; Pickett et al. 1998]. Although this line is much weaker than the millimeter wave lines, it allows the retrieval of the ozone mixing ratio to higher altitudes, because the Doppler width is reduced by a factor of 10. In addition, the atmospheric opacity, which is mainly due to water vapor, is much lower at 11 GHz, so observations can be made at low altitude sites under almost all weather conditions.

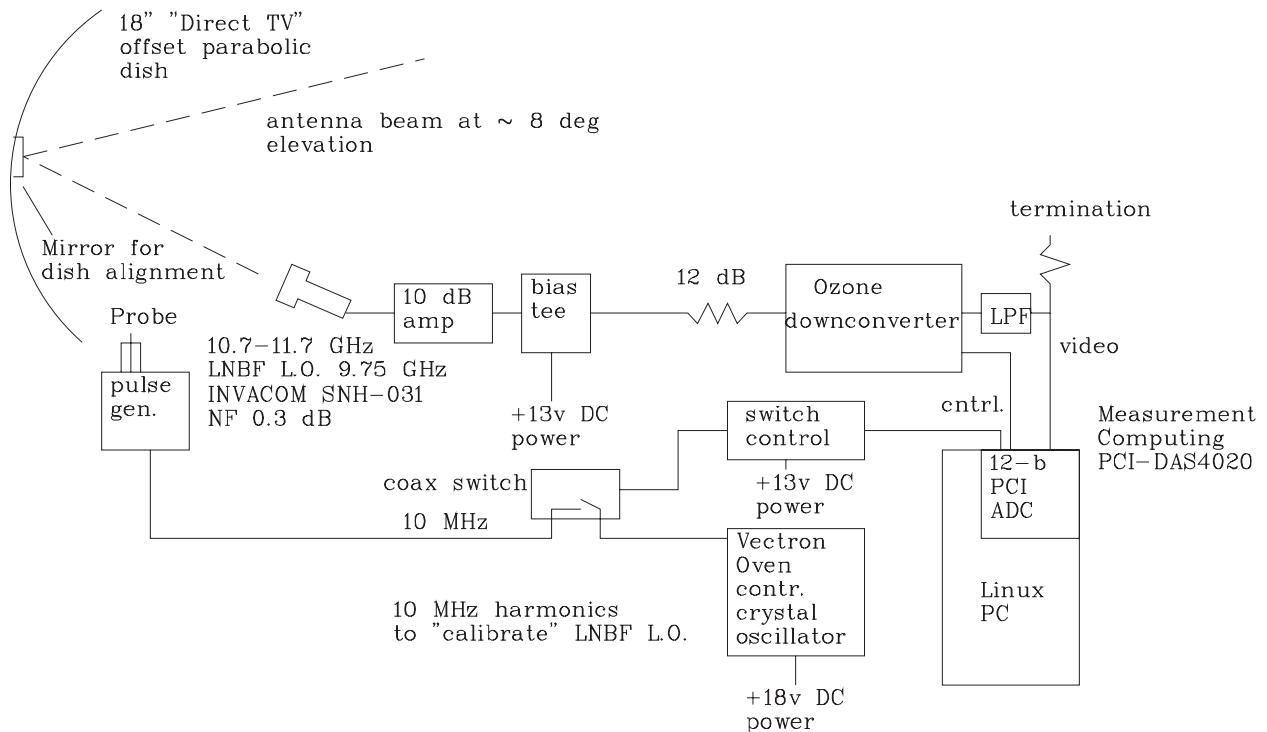
Furthermore, the radiometers in the 11-GHz band can be constructed from very inexpensive satellite television low noise block downconverters (LNBF), because the 10.7–11.7-GHz band is allocated to fixed and fixed-satellite service. Although we report on observations made from Chelmsford High School (CHS; 42.62°N, 71.37°W) and the Massachusetts Institute of Technology (MIT) Haystack Observatory (42.61°N, 71.49°W) looking in a fixed direction, there is potential for improved geographical coverage and better signal-to-noise ratio with an expanded network.

---

\* Current affiliation: Raytheon Integrated Defense Systems, Billerica, Massachusetts.

---

Corresponding author address: A. E. E. Rogers, MIT Haystack Observatory, Route 40, Westford, MA 01886.  
E-mail: arogers@haystack.mit.edu



Setup to observe the 11.0724545 GHz ozone line

FIG. 1. Setup to observe the 11.072 454 5-GHz ozone line.

## 2. 11-GHz ozone radiometer

Our observing technique is similar to that used for other ground-based ozone radiometers (Zommerfelds et al. 1989), with a few exceptions:

- (i) A fixed beam of  $4^\circ$  full width at the half power points is employed instead of beamswitching. The radiometer is manually calibrated by placing an ambient temperature absorber in front of the antenna.
- (ii) Frequency calibration is performed by periodic injection of a calibration signal from a stable calibrated oven crystal oscillator in order to correct for the drifts in the unstabilized local oscillator in the LNBF.

Figure 1 shows the schematic block diagram of the radiometer. The dish is located at  $42.62^\circ\text{N}$ ,  $71.37^\circ\text{W}$  and points at an azimuth of  $172^\circ$  and elevation of  $8^\circ$  to intersect the atmospheric layer at 100-km altitude at  $37.8^\circ\text{N}$ ,  $70.5^\circ\text{W}$ . In July 2008, a second system was added at the MIT Haystack Observatory that was pointed to intersect the atmospheric layer close to the same location. The oven crystal provides a 10-MHz reference for the downconverter and a pulse generator. In addition to observing the ozone line, the spectrometer periodically

observes the 1107th harmonic of the pulses, which have a risetime of a few ps, at 11.07 GHz to correct the spectra for the drift in the local oscillator in the LNBF. Because the drift in the local oscillator is driven by slow temperature changes in the LNBF, a correction once every minute was adequate to keep the frequency within 1 kHz. The oven crystal's long-term drift is less than  $100 \text{ ppb yr}^{-1}$ .

## 3. Observing technique

The spectrometer uses a 12-bit analog-to-digital sampling card running at a  $20 \text{ Msample s}^{-1}$  rate. Fast Fourier transforms of 4096 samples in length are performed in software to derive a 10-MHz-wide spectrum with 4.9-kHz resolution. Subsequently, the resolution is smoothed to 9.8 kHz and only the central 1.25-MHz bandwidth, which is well within the flat region of the analog filters in the downconverter, is used for the ozone line. To minimize systematic effects, frequency switching is used to obtain a difference spectrum with the ozone line centered in the lower quarter band and then inverted in the center of the upper three-quarter band. Following an accumulation of 90 s, the upper-half-band spectrum is subtracted from the lower-half-band spectrum and a 625-kHz band centered on the ozone line is

stored to disk for subsequent averaging. The theoretical noise in the spectrum is

$$\Delta T_{\text{rms}} = T_s 2^{1/2} (bt)^{-1/2},$$

where

$$\begin{aligned} T_s &= \text{system noise temperature } (\sim 100 \text{ K}), \\ b &= \text{resolution } (9.8 \text{ kHz}), \text{ and} \\ t &= \text{total integration time } (\text{s}). \end{aligned}$$

Frequency switching results in a factor of  $\sqrt{2}$  increase in the noise compared with an unswitched spectrometer. For 24 h, the root-mean-square (rms) noise is 5 mK. The spectrometer was calibrated by manually placing an absorbing vane in front of the LNBF. The system noise is about 100 K, which contains contributions of about 30, 30, and 40 K from the low noise amplifier, atmosphere, and antenna spillover losses, respectively. The system noise calibration is only performed about once every 3 months. However, the changes are mostly in the contribution of the atmosphere of about 30 K, which can be as high as 50 K in humid conditions and as low as 15 K when water vapor in the atmosphere is a minimum. To some extent, we can correct for these changes from the changes in total power. In the future, an automated method of system noise calibration using a calibrated noise source generator will be implemented.

The ozone concentrations for two regions, one above and one below 80 km, were retrieved by fitting a two-parameter model to the observed spectra. Figure 2 shows the averaged spectrum from 30 days of nighttime data along with a linear least squares fit based on a linear combination of ozone from the two regions. The first is a region from 50 to 80 km, with constant volume mixing ratio, and the second is a region from 80 to 104 km, which has a Gaussian distribution of the ozone mixing ratio with altitude, centered at 92 km, with a full width at half maximum of 10 km. A line strength of  $-6.9997$ , corrected for temperature, is used from the JPL tables (Pickett et al. 1998). For the model spectrum, the regions below and above 80 km were assumed to have constant temperatures of 210 and 175 K, respectively. Also, a fixed relation between pressure and altitude with 0.001 hPa at 92 km was assumed. In addition, a collision line width (half width at half maximum) of  $2.6 \text{ MHz hPa}^{-1}$  at 296 K with 0.71 temperature coefficient was taken from the 2004 High-Resolution Transmission Molecular Spectroscopic Database (HITRAN04; Rothman et al. 2005). The Doppler line width was calculated assuming kinetic temperatures of 210 K below 80 km and 175 K above 80 km. Varying the assumed temperature below an 80-km altitude by up to 50 K makes very little difference to the model, because only the wings of the line are affected.

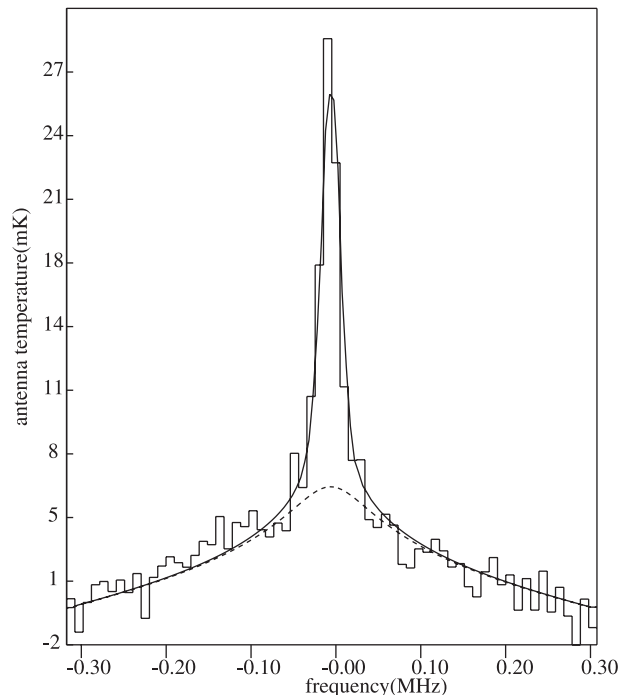


FIG. 2. Spectrum from observations at night at CHS taken from 26 Jan through 31 May 2008. The line center is at 11.072 454 5 GHz. The solid curve is the model fitted to the data. The dashed curve and the difference between the solid and the dashed curves are the portions of the model for the ozone below and above 80 km, respectively.

The assumed temperature above 80 km, on the other hand, has a somewhat larger effect, because it changes the Doppler width. Although the assumed temperatures do not have much effect on the line shape, they have a more significant effect on the ability to accurately estimate the ozone concentration. The error in the ozone contributions from these two regions were obtained from the covariance matrix, assuming the theoretical noise in the spectrum. This simple retrieval method was chosen over the iterative radiative transfer method of Chahine (1972), because the 11-GHz line is optically thin. The choice of only two regions was the result of the poor signal-to-noise ratio, owing to the weakness of the line. The signal-to-noise ratio was optimized by choosing an antenna beam elevation to maximize the ratio of pathlength to system noise. This elevation is close to  $8^\circ$  for an ozone layer at 92-km altitude, taking into account the curvature of the earth and the atmospheric attenuation at 11 GHz.

#### 4. Diurnal variations

Figure 3 shows the diurnal variations of the ozone mixing ratio for the two regions for data taken from January through October 2008. The data are plotted as a function of local time. To account for the changes in sunrise and sunset times over the long time span of the

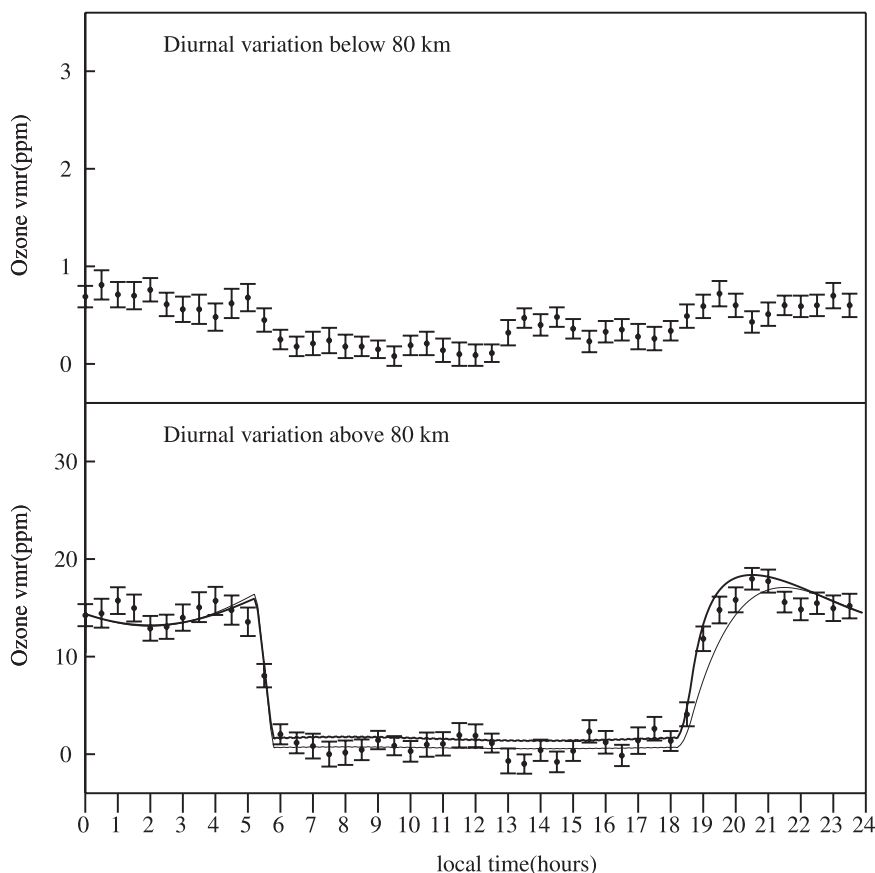


FIG. 3. Diurnal variations in the ozone vmr for regions below and above 80 km from observations at 11 GHz taken from 26 Jan through October 2008. Data collected from 26 Jan to 2 Jul were from CHS, whereas data collected after 2 Jul were from both CHS and a site at MIT Haystack Observatory. The error bars are  $\pm 1\sigma$ , calculated from the covariance matrix based on the theoretical noise of the spectrometer. The solid curve is fit to the data using a simple model based on the method given by Smith and Marsh (2005). The thin line curve is the same model shifted to a higher altitude. These models and the best-fit parameters are given in section 7 of the text.

data, local time was taken to be 6 and 18 h at sunrise and sunset, respectively. Each data point is obtained from the average of all the spectra (from January through October 2008) within a window of 1 h ( $\pm 30$  min from local time). A model that is fitted to the diurnal variations above 80 km is also shown, which we discuss in section 7. The stability of the radiometer system is judged to be good enough so that the relative measurements should be accurate to within 10%, because the changes in atmospheric opacity are small at 11 GHz. Data with high system noise due to rain or a wet LNBF have been excluded from the averages. Absolute accuracy of the measurements, which depends on the calibration, is estimated to be about  $\pm 30\%$  in the total integrated ozone above 80 km for the assumed fixed temperature of 175 K, because the instrument is directly sensitive to the product of the integrated ozone column

and ozone temperature. An altitude of 92 km was chosen for the peak of the ozone, because it provides the best fit to the data and is consistent with the altitude of the peak of the ozone at midlatitude found by other techniques. If the peak is moved to a significantly lower altitude, the model spectrum is too broad to fit the data. Because the values of ozone mixing ratio above 80 km are dependent on the assumed altitude and width of the Gaussian distribution used to derive the fitted spectrum, moving the peak to a higher altitude would have resulted in higher mixing ratios. However, the factor by which the ozone vmr increases at night shown in Fig. 3 would not change.

From Fig. 3, it is clear that the ozone mixing ratio above 80 km starts to decline about 30 min before sunrise at ground level and declines rapidly in less than 1 h. The start of the decline before sunrise is expected, because the sun's rays reach the mesopause about

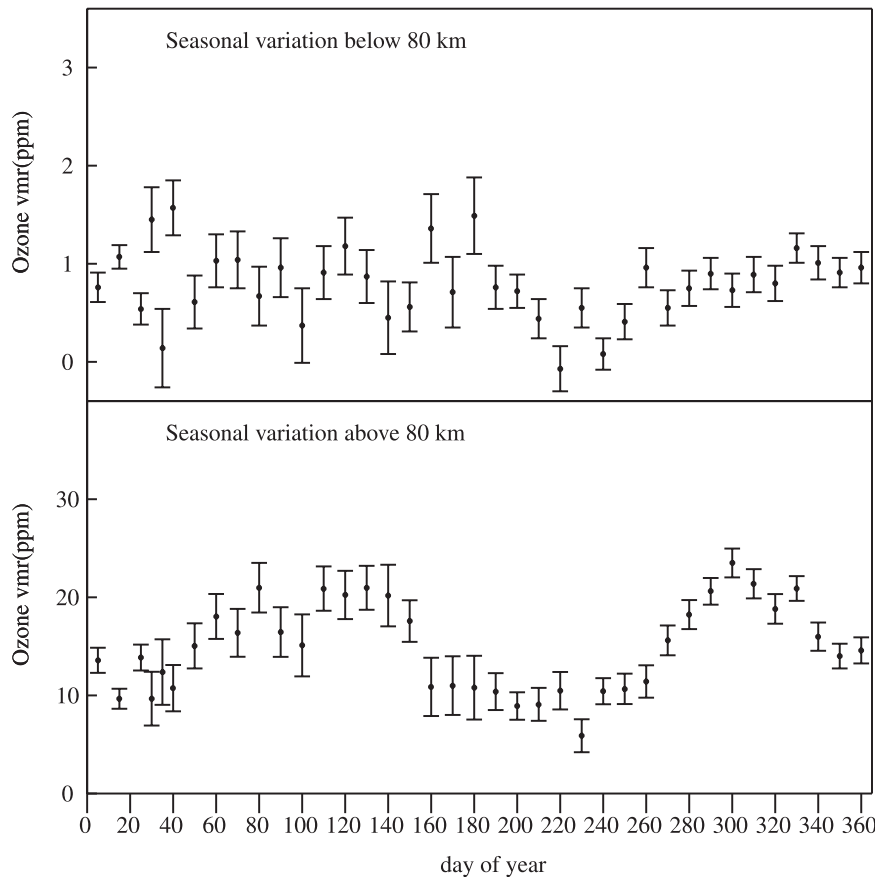


FIG. 4. Seasonal variations in ozone from 26 Jan 2008 through 26 Jan 2009 for regions below and above 80 km obtained from 10-day averages plotted every 10 days for nighttime data for when the sun was below  $-10^\circ$  elevation. The error bars are  $\pm 1\sigma$ . From 3 Jul 2008 (day 185), the data are the average of the spectrometers at CHS and Haystack Observatory. As a result, the data after day 185 have smaller error bars.

40 min before sunrise. The ozone above 80 km takes about 1 h following sunset at ground level to reach the nighttime level. The diurnal variations below 80 km are more gradual. The ratio of the nighttime to daytime ozone mixing ratios is lower than the corresponding ratio above 80 km. The nighttime ozone above 80 km also shows significant semidiurnal variation, which fits the variation expected from a semidiurnal variation in the temperature reported by States and Gardner (2000).

## 5. Seasonal changes

The best-fit nighttime ozone volume mixing ratios for 10-day averages are plotted in Fig. 4 for the regions below and above 80 km. The ozone above 80 km shows a significant semiannual trend of increased ozone around the time of the spring and fall equinoxes, which is consistent with the model of Smith and Marsh (2005). This model, known as the ROSE model, is a 3D global model based

on the primitive equations with interactive chemistry. The ROSE model predicts the ozone concentration at night from the balance between the creation by collisions of atomic oxygen with molecular oxygen and a third catalytic molecule, such as nitrogen, and the destruction by reactions with atomic hydrogen. The seasonal change is mainly the result of the seasonal variation in the atomic hydrogen (Thomas 1990). Lossow et al. (2008) show a clear semiannual variation in water vapor, suggesting that the seasonal variation of atomic hydrogen is largely due to the seasonal variation of water vapor. Above 80 km, the water vapor peaks at the summer solstice with minima at the equinoxes and a lower peak at the winter solstice. Lossow et al. (2008) suggest that this variation is produced by the interhemispheric meridional circulation, which we suggest may also have a significant influence on the nighttime ozone above 80 km.

The plot of the ozone above 80 km shows a marginally significant ( $\sim 2\sigma$ ) dip below the otherwise smooth

seasonal variation centered at day 100 (9 April 2008), which could have been the result of an injection of protons from the magnetosphere that occurred from 6 to 10 April 2008, when earth was within a solar wind stream from a coronal hole reported by the Solar and Heliospheric Observatory (SOHO) extreme ultraviolet (UV) telescope. Another similar event occurred 15–19 August 2008, accompanied by another marginally significant dip centered on day 230 (17 August 2008). Large injections of energetic protons in “proton events” have been shown by Verronen et al. (2005, 2006) to result in large reductions of ozone at the “tertiary maximum” centered at about 75 km. Although the modest injection in April 2008 was probably not sufficient to have a major effect on the ozone, we suggest the smaller events, especially those spread over several days, could result in joule heating of the region above 80 km, as seen by Roble et al. (1987), with a consequent reduction of ozone resulting from a increase in the reaction of ozone with atomic hydrogen. A temperature increase of 20 K is estimated to result in a reduction of the ozone by about a factor of 2, as shown by Smith and Marsh (2005).

## 6. Comparison with other data

The approximately 1-h rise and <1-h fall times for the ozone mixing ratio above 80 km are in general agreement with the observations of Zommerfelds et al. (1989) for 74 km. The phasing relative to sunrise and sunset is also in agreement when the actual sunrise and sunset times are taken into account. Zommerfelds et al. (1989) plot their data versus time of day, whereas we have plotted the data versus local time defined to make 6 and 18 h the times of sunrise and sunset, respectively, independent of the time of year.

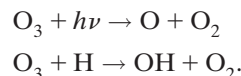
We obtained a night–day ratio of  $15_{-5}^{+30}$  ( $1\sigma$ ) for the ozone above 80 km. This is consistent with the trend in the data of Zommerfelds et al. (1989), which shows an increase in the night–day ratio with increasing altitude up to a value of about 6 at 74 km.

Sounding of the Atmosphere using Broadband Emission Radiometry (SABER; Huang et al. 2008) has measured semiannual changes in the ozone up to 100-km altitude with amplitudes of a few ppm or greater, which shows increased ozone in the months of April and May. Recent measurements by SABER (Smith et al. 2008) show mixing ratios over 20 ppmv at the equinoxes. This is consistent with the increased ozone we derive from our measurements in April and May and again in October and November.

## 7. Comparison with chemical models

We have compared our results with a simplified model based on the model of ozone in the mesopause region

given by Smith and Marsh (2005). They show that the dominant processes that destroy ozone in the region above 80 km are ultraviolet radiation and collisions with atomic hydrogen:



The only process that produces ozone is the collisions of atomic oxygen and molecular oxygen along with a third body, such as nitrogen:



During the daytime, the ultraviolet destruction rate plus the destruction by hydrogen is balanced by the 3-body creation rate, whereas at night the destruction by hydrogen collisions is balanced by the 3-body creation rate. The continuous curve in the Fig. 3 (bottom) compares our diurnal variations for the region above 80 km with a simplified model based on the method of Smith and Marsh (2005).

This model assumes the reaction rate given in Eqs. (7) and (9) of Smith and Marsh (2005) of

$$k_1 = 6.0 \times 10^{-34} \left( \frac{300}{T} \right)^{2.4}$$

for the creation of ozone and

$$k_3 = 1.4 \times 10^{-10} \exp\left(\frac{-470}{T}\right)$$

for the destruction of ozone by collisions with atomic hydrogen. Mixing ratios of  $1.1 \times 10^{-2}$  and  $1.4 \times 10^{-6}$  were chosen for atomic oxygen and hydrogen, respectively. These mixing ratios, which result in a model that fits the data quite well, are close to those of Smith and Marsh (2005) for the month of March at 37°N. A pressure of 0.001 hPa, which corresponds to an altitude of about 92 km, was chosen as being representative of the peak of the ozone mixing ratio. To be able to average data throughout the year, local time was defined relative to 6 and 18 h for local sunrise and sunset, respectively. The UV was turned on at 5.5 h and off at 18.5 h to approximate the sun’s illumination at 92 km. The UV was assumed to destroy the ozone at a rate of  $10^{-2}$ . The detailed model of Smith and Marsh [2005, their Fig. (5)] accurately accounts for the UV illumination via the radiative transfer through the layers of the atmosphere.

Equating the creation rate to the destruction rate and solving the differential equation results in an equilibrium nighttime mixing ratio of ozone  $\text{O}_{3_{\text{vmr}}}$  of

$$\text{O}_{3_{\text{vmr}}} = \frac{k_1 \times \text{O}_2_{\text{vmr}} \times \text{O}_{\text{vmr}} \times \rho}{k_3 \times H_{\text{vmr}}}$$

TABLE 1. Model calculations for the nighttime equilibrium and the ozone recovery time constant.

$O_{3_{\text{vmr}}}$ (ppm)	$\tau$ (s)	$O_3$ density ( $\text{cm}^{-3}$ )	Temp (K)	Pressure (hPa)
30.4	2263	$1.4 \times 10^9$	155	0.001
15.2	4528	$3.6 \times 10^8$	155	0.005
14.2	1807	$5.9 \times 10^8$	175	0.001
7.1	3618	$1.5 \times 10^8$	175	0.005

and a time constant  $\tau$  for the recovery of the ozone following the extinction of the UV of

$$\tau = \frac{1}{(k_3 \times H_{\text{vmr}} \times \rho)},$$

where  $\rho$  is the “background” number density. The calculated results for nighttime equilibrium and time constant are given in Table 1. The thick solid curve that is fitted to the diurnal variation in Fig. 3 is the time-dependent model for a pressure of 0.001 hPa and a temperature of 175 K. To improve the fit, a semidiurnal cosine wave of 10 K peak to peak with a maximum at 2 h was added. An increase in temperature decreases the ozone concentration significantly through the strong temperature dependence of the reaction rates. This diurnal temperature variation is close to that reported by States and Gardner (2000). The thin curve in Fig. 3 is a second model fit based on increasing the altitude of the ozone peak from 92 to 97 km (0.0005 hPa) and decreasing the temperature to 155 K to match the observed ozone concentration. This second model does not fit the data at sunrise because of the increased time constant for the restoration of the ozone at night suggesting that the ozone peak is below 97 km. Unfortunately, the spectra themselves are insufficiently sensitive to altitude to allow a determination of the altitude, because above 90 km the pressure broadening becomes negligible, resulting in a mainly Doppler broadened line. This is the weakness of the ground-based spectrometer compared with the satellite limb scanning instrument, such as SABER, which can determine the altitude from the scan angle. However, if the chemistry model is accurate, then the ozone altitude can be indirectly determined from the time constant associated with recovery of the mesospheric ozone at sunrise. For example, it should be possible to verify the high ozone mixing ratios at the equator reported by Smith et al. (2008), which occur at an altitude around 97 km, by making 11-GHz observations at the equator. The observations should show an increase in the ozone recovery time at sunrise to more closely fit the second diurnal variation model shown in Fig. 3.

Smith and Marsh (2005, their Figs. 2, 3) show seasonal variations from the ROSE model for the equator and a latitude of 55°N; both of their figures follow the same trend, as seen in our measurements plotted in Fig. 4. If we ignore scale errors and consider only the ratio of ozone, interpolated to a latitude of 38°N and averaged over an altitude range of 80–100 km, both the model and our data show an approximate doubling of the ozone at the peak in April and May and again in October and November compared with the ozone in January, February, and July.

## 8. Conclusions

The 11-GHz line of ozone can be observed with a simple low-cost spectrometer, and the observations can be used to learn more about the ozone in the upper mesosphere and lower thermosphere. Extended coverage could be achieved by deploying spectrometers worldwide. The signal-to-noise ratio could be improved by adding independent channels through the use of dual polarization and multiple antennas.

The seasonal variation of ozone above 80 km derived from the measurements obtained so far is reasonably consistent with the ROSE model of Smith and Marsh (2005). The diurnal variations show evidence for the semidiurnal tide, and the ozone recovery time at sunset is consistent with a simplified chemical model for which the ozone mixing ratio has a maximum at 0.001 hPa.

*Acknowledgments.* This work was supported in part by the National Science Foundation Grant DUE-0535839 and in part by MIT. We acknowledge the contributions by Dr. Anne K. Smith of the Atmospheric Chemistry Division, National Center for Atmosphere Research, Boulder, Colorado, to our understanding of the chemistry of ozone in the mesopause region. We thank the students and staff of Chelmsford High School for their contributions in the acquisition of the data. We thank the reviewers for making us aware of the HITRAN database for the estimate of the pressure broadening of the 11.07-GHz line, as well as for suggesting several improvements to the manuscript. We also thank John Foster of the Atmospheric Sciences group of the Haystack Observatory for helpful discussion of the potential effects of space weather on ozone.

## REFERENCES

- Chahine, M. T., 1972: A general relaxation method for inverse solution of the full radiative transfer equation. *J. Atmos. Sci.*, **29**, 741–747.
- Huang, F. T., H. G. Mayr, C. A. Reber, J. M. Russell III, M. G. Mlynczak, and J. G. Mengel, 2008: Ozone quasi-biennial oscillations (QBO), semiannual oscillations (SAO), and correlations with temperature in the mesosphere, lower thermosphere,

- and stratosphere, based on measurements from SABER on TIMED and MLS on UARS. *J. Geophys. Res.*, **113**, A01316, doi:10.1029/2007JA012634.
- Lobsiger, E., and K. F. Künzi, 1986: Night-time increase of mesospheric ozone measured with ground-based microwave radiometry. *J. Atmos. Terr. Phys.*, **48**, 1153–1158.
- Lossow, S., J. Urban, J. Gumbel, P. Eriksson, and D. Murtagh, 2008: Observations of the mesospheric semi-annual oscillation (MSAO) in water vapor by Odin/SMR. *Atmos. Chem. Phys.*, **8**, 6527–6540.
- Pickett, H. M., R. L. Poynter, E. A. Cohen, M. L. Delisky, J. C. Pearson, and H. S. P. Muller, 1998: Sub-millimeter, millimeter, and microwave spectral line catalog. *J. Quant. Spectrosc. Radiat. Transfer*, **60**, 883–890.
- Roble, R. G., and Coauthors, 1987: Joule heating in the mesosphere and thermosphere during the July 13, 1982, solar proton event. *J. Geophys. Res.*, **92**, 6083–6090.
- Rothman, L. S., and Coauthors, 2005: The HITRAN 2004 molecular spectroscopic database. *J. Quant. Spectrosc. Radiat. Transfer*, **96**, 139–204.
- Smith, A. K., and D. R. Marsh, 2005: Processes that account for the ozone maximum at the mesopause. *J. Geophys. Res.*, **110**, D23305, doi:10.1029/2005JD006298.
- , —, J. M. Russell III, M. G. Mlynczak, F. J. Martin-Torres, and E. Kyrölä, 2008: Satellite observations of high nighttime ozone at the equatorial mesopause. *J. Geophys. Res.*, **113**, D17312, doi:10.1029/2008JD010066.
- States, R. J., and C. S. Gardner, 2000: Thermal structure of the mesopause region (80–105 km) at 40°N latitude. Part II: Diurnal variations. *J. Atmos. Sci.*, **57**, 78–92.
- Thomas, R. J., 1990: Atomic hydrogen and atomic oxygen density in the mesopause region: Global and seasonal variations deduced from solar mesosphere explorer near-infrared emissions. *J. Geophys. Res.*, **95**, 16 457–16 476.
- Verronen, P. T., A. Seppälä, M. A. Clilverd, C. J. Rodger, E. Kyrölä, C.-F. Enell, T. Ulich, and E. Turunen, 2005: Diurnal variation of ozone depletion during the October–November 2003 solar proton events. *J. Geophys. Res.*, **110**, A09S32, doi:10.1029/2004JA010932.
- , —, E. Kyrölä, J. Tamminen, H. M. Pickett, and E. Turunen, 2006: Production of odd hydrogen in the mesosphere during the January 2005 solar proton event. *Geophys. Res. Lett.*, **33**, L24811, doi:10.1029/2006GL028115.
- Wilson, W. J., and P. R. Schwartz, 1981: Diurnal variations of mesospheric ozone using millimeter-wave measurements. *J. Geophys. Res.*, **86**, 7385–7388.
- Zommerfelds, W. C., K. F. Künzi, M. E. Summers, R. M. Bevilacqua, D. F. Strobel, M. Allen, and W. J. Sawchuck, 1989: Diurnal variations of mesospheric ozone obtained by ground-based microwave radiometry. *J. Geophys. Res.*, **94**, 12 819–12 832.